Electrochimica Acta 424 (2022) 140624

Contents lists available at ScienceDirect

Electrochimica Acta

journal homepage: www.journals.elsevier.com/electrochimica-acta

A high power density solid electrolyte based on polycaprolactone for high-performance all-solid-state flexible lithium batteries

Yuhang Li [a], Fang Wang [a], Boyuan Huang [b], Can Huang [a], Dexuan Pei [a], Zixian Liu [a], Shuoguo Yuan [a,*], Shuen Hou [a], Guozhong Cao [c], Hongyun Jin [a,*]

[a] Engineering Research Center of Nano-Geomaterials of Ministry of Education, Faculty of Materials Science and Chemistry, China University of Geosciences, Hongshan Road Lumo, Wuhan 430074, China
[b] Department of Materials Science and Engineering, Southern University of Science and Technology, Shenzhen, Guangdong 518055, China
[c] Department of Materials Science & Engineering, University of Washington, WA 98195, USA

ARTICLE INFO

Keywords:
All-solid-state lithium battery
Composite polymer electrolytes
High power density
Li-ion transference number
Faster discharging

ABSTRACT

All-solid-state lithium batteries (ASSLBs) have been regarded as the next-generation battery technology owing to the superiority of safety, potentially high enetgy density and long cycling life. However, the slow charging limitations of ASSLBs hinder their practical applications. To tackle this issue, composite polymer electrolytes (CPEs) based on polycaprolactone (PCL) are developed to achieve satisfactroy enhancements for charging/discharging performances of ASSLBs. The addition of ceramic powder in PCL-based CPEs suppresses the crystallization of PCL and at the same time enhances the Li-ion transport behaivor. The present ASSLBs within PCL-based CPEs display excellent cycling performance with the initial discharge specific capacity of 108.2 mAh g^{-1}, as well as good capacity retention of 75% after 500 cycles at a current density of 2 C at 55 °C. The high performance of ASSLBs is attributed to the high Li-ion transference number of 0.8 and excellent interfacial stability and wettability originated from the addition of ceramic components. It is demonstated that the PCL-based CPEs exhibit high Young's Modulus (2.8 GPa) and to the long-term cycling stability of ASSLBs. This study opens up new possibilities for the development of fast-charging batteries with an emphasis on the design of new polymer electrolytes.

1. Introduction

Safe and high energy density electrical energy storage devices are urgently needed to meet the demand of the rapid growth of electric vehicles (EVs), hybrid electric vehicles (HEVs) and smart grids [1–4]. Rechargeable Li-ion batteries (LIBs) are crucial for developing many smart applications and have attracted widely attention. But there are three issues arising from liquid organic electrolytes that hinders the better performance of LIBs [5–8]. Firstly, the thermal instability, volatility, toxicity and flammability of commercial liquid organic electrolytes are pivotal problems that can cause serious safety concerns such as fire and explosion [9–11]. Secondly, lithium dendrite formation due to inhomogeneous charging of the anode can cause short circuit in liquid organic electrolytes based LIBs [12–14]. Last but not least, it is challenging to achieve a fast charging/discharging ability, which is desired for practical application. For example, LIBs of EVs or HEVs are required to discharge at high rates immediately when starting or accelerating. Although current liquid organic electrolytes offer high conductivity, but they have a Li-ion transference number (t_{Li}^{+}) below 0.5, indicating that the majority of the total ionic conductivity is in fact the result of anion motion [15]. The low t_{Li}^{+} causes large concentration gradient so that the rate of charging/discharging has to be reduced to preserve battery life, thus seriously limiting its power and energy density [16].

Over the past decade, significant research efforts have been devoted to develop high power density for fast charging LIBs. To this end, an ideal electrolyte is supposed to simultaneously meet good mechanical properties, high t_{Li}^{+} and ionic conductivity. Lithium dendrite growth can be mechanically blocked if the modulus of the electrolytes is about twice that of lithium metal [17]. Therefore, it is meaningful to develop high Young's Modulus yet flexible battery separators to meet the stringent demands in the future lithium battery technologies [18]. Improved Young's Modulus of electrolytes materials at the interface allows for better resistance and wettability against dendrite formation and thus promotes stability for all-solid-state lithium batteries (ASSLBs) [19,20].

* Corresponding authors.
E-mail addresses: yuanshuoguo@cug.edu.cn (S. Yuan), jinhongyun@cug.edu.cn (H. Jin).

https://doi.org/10.1016/j.electacta.2022.140624
Received 20 December 2021; Received in revised form 19 March 2022; Accepted 24 May 2022
Available online 25 May 2022

Besides, high t_{Li}^{+} and ionic conductivity can avoid the cumulation of mobile anions near the electrode, which may not only cause the concentration polarization, but also take part in unwanted reactions resulting in a reduced active area of the electrode.

Currently, several studies have devoted to single-ion conducting polymer electrolytes, which possess high $t_{Li}^{+}\geq 0.9$ and obtained excellent battery performance. But some of them need very complicated process from preparation to purification, remarkably impeding their commercialization [21]. On one hand, inorganic solid electrolytes (ISEs) possess a high Li-ion transference number ($t_{Li}^{+}\approx 1$) and high ionic conductivities, but the ISEs have poor interfacial contact with electrodes which have inhibited their practical applications in commercial LIBs [22,23]. On the other hand, organic solid-state electrolytes or solid polymer relectrolytes (SPEs) have shown good interfacial contact with electrodes, but can not reveal significant Li-ion transference number and ionic conductivities. It is the expedient process to develop CPEs to synergistically combine the beneficial properties of both ISEs (high t_{Li}^{+} and mechanical strength) and SPEs (good interfacial properties and flexibility) [24–26]. Zhang et al. have fabricated the composite polymer electrolyte (CPEs) based on polyethylene oxide (PEO), t_{Li}^{+} of 0.46, which exhibited the excellent flexibility, and good capacity retention of 90% after 200 cycles at 0.1 C, 60 °C [27]. Additionally, the PEO based solid state electrolyes (SSEs) have been investigated for nearly 50 years and obtained excellent performance on ASSLBs [28–31], which have been commercialized and used in the Bolloré Bluecar [32]. As an alternative to PEO, polycaprolactone (PCL) has carbonyl groups (=O) and ethyoxyl (EO) groups that are the key for forming O-Li^{+} coordination mode in CPEs system, which is biodegradable, environmental friendly and low cost for large-scale production. Moreover, Fonseca et al. fabricated the SSEs based on PCL/$LiClO_4$ to develop biodegradable electrolyte in ASSLBs for the first time in 2006 [33]. Eriksson et al. proposed the CPEs composed of PCL/LiTFSI/Al_2O_3, which displayed good performance in ASSLBs in 2019 [34]. In addition, the excellent performance SSEs that based on the copolymer of PCL are studied [35–38]. Unfortunately, to the best of our knowledge, there is still no experimental report on CPEs possessing the ability of rapid charging/discharging (≥2 C).

Above experimental and theoretical studies revealed that the use of CPEs with high Young's Modulus and high t_{Li}^{+} is one of the most promising approaches to achieve high performance ASSLBs with rapid charging/discharging kinetics. This paper reports the design and fabrication of a new electrolyte system as CPEs where $Li_{1.4}Al_{0.4}Ti_{1.6}(PO_4)_3$ (LATP) and LiTFSI are both filled in the polycaprolactone (PCL) matrix. The optimized PCL-LiTFSI-LATP CPEs (hereafter abbreviated as "PCL-based CPEs") have high t_{Li}^{+}=0.8 ensuring the superior rate capability, cycling stability and suppressing lithium dendrite growth. Without any liquid electrolyte, the ASSLBs based on $LiFePO_4$ (LFP) present a high initial discharge specific capacity of 108.2 mAh g^{-1} at 2 C (≈0.29 mA cm^{-2}), 55 °C, and shows excellent cycling performance without distinct lithium dendrites growth after 500 cycles at 2 C with 75% capacity retention.

2. Experimental section

2.1. Materials preparation

Lithium bis(trifluoromethylsulphonyl)imide (LiTFSI), PEO (Mw: 600,000) and PCL (Mw: 55,000) was dried under vacuum at room temperature for 24 h before use. Powders of TiO_2, $(NH_4)_2HPO_4$, Li_2CO_3, Al_2O_3, and dimethyl carbonate (DMC) were purchased from the Aladdin, shanghai (China). The cathode material LFP and lithium metal were obtained from China Energy Technology Co. Ltd. The cathode materials and conducting agent were dried in a vacuum oven for 12 h at 60 °C. The LATP was synthesized by TiO_2, $(NH_4)_2HPO_4$, Li_2CO_3, Al_2O_3 with a conventional solid solution method [39]. PCL and LiTFSI were dissolved in anhydrous DMC by magnetic stirring for 6 h at 55 °C, and the O/Li was controlled by the molar ratio at 20. Then, the LATP particle contents of 40 wt % were added as active fillers into the solution, and the solution continued to be stirred for 6 h at 55 °C to disperse homogeneously (Based on the results of our previous experiments, we confirmed the 40 wt% LATP was reasonable for PCL-based CPEs) [7]. Simultaneously, the same preparation technology was used for PEO-LiTFSI-LATP CPEs (hereafter abbreviated as "PEO-based CPEs") to compare the perfomance of PCL-based CPEs, which was helpful to evaluate the PCL-based CPEs application prospect realistically and objectively. Subsequently, the obtaining viscous slurry was casted onto the glass plate by coater (PEO-based CPEs used stainless steel plate) and was further dried at room temperature overnight to yield CPEs. Afterwards, the membrane of CPEs was cut into circular rounds with a diameter of 19 mm (The thickness of CPEs membrane was ~80 μm), and stored in an Ar-filled glove box for the next characterization measurement and assembly ASSLBs.

2.2. Materials characterizations and electrochemical measurements

The morphologies and element distribution of CPEs membranes were characterized by SEM (HITACHI SU8010) and EDS. The particle size LATP powder and the obtained CPEs membranes were examined using $CuK_{\alpha 1}$ radiation (λ = 0.15405 nm) with a D8-ADVANCE XRD. The $Li_{1.4}Al_{0.4}Ti_{1.6}(PO_4)_3$ (LATP) was prepared by a conventional solid solution method, and the phase compositions were examined by XRD, as shown in Fig. S1a. The thickness of LATP plate was 1 mm, and the diameter was 11 mm.The ion conductivity of LATP was 7.07×10^{-4} S cm^{-1} (Room temperature, RT) and the EIS was exhibited in Fig. S1b. The TGA was characterized on a STA 449 F3 Thermal Analyzer with a heating rate of 10 ºC min^{-1} from room temperature to 900 °C in nitrogen atmosphere. DSC characterizations were operated to explore the χ_c for different electrolyte membranes and the T_m of samples under a flowing nitrogen atmosphere. The ionic conductivities of CPEs were investigated by EIS. The cathode was prepared according to coating process for ASSLBs. The active materials (LFP), carbon black (Super-P) and polyvinylidene fluoride (PVDF) (60: 20: 20 by weight) were coated on an aluminum foil. Then the coated cathode was dried in vacuum at 60 °C for 24 h to remove the remaining N-methylpyrrolidinone solvent. The lithium metal was served as anode with a diameter of 16 mm. The LFP cathode was cut into circular rounds with a diameter of 15 mm in order to be efficiently used, and the loading density of active material was controlled at 0.90~1.20 mg cm^{-2}. The ASSLBs based on CPEs were assembled in an Ar-filled glove box (CR 2032-type). The cycling performance and rate capability (0.2~2 C) of the ASSLBs were investigated by Land CT2001A battery testing system at 55 °C with the voltage range of 2.5~4.2 V (vs. Li/Li^{+}). The resistance of ASSLBs was investigated in the frequency range from 10 M Hz to 0.1 Hz using a Zahner electrochemical workstation at 55 °C. The Young's Modulus was measured by AFM (Asylum Research MFP-3D) at room temperate.

3. Results and discussion

3.1. Schematic illustration of designed PCL-based CPEs

Our design concept of ASSLBs with PCL-based CPEs is shown in Fig. 1a. The SEM image of the PCL-based CPEs with LATP particles is exhibited in Fig. 1b. The cross section morphology of the PCL-based CPEs show that the LATP particles are homogeneously dispersed and embedded in the PCL matrix. The TGA curves of PCL, PEO, PCL-based CPEs and PEO-based CPEs are exhibited in Fig. S2a-c. PCL-based CPEs do not show an obvious weight loss until 300 °C (Fig. S2c), indicating that the PCL-based CPEs have not significant deterioration at the elevated temperature up to 300 °C, which completely satisfies the working requirements of LIBs. The PCL-based CPEs could operate in more extreme environments than liquid organic electrolytes without security risks because of superior thermal stability. Besides, the PEO-based CPEs also have shown remarkable thermal stability (Fig. S2c),

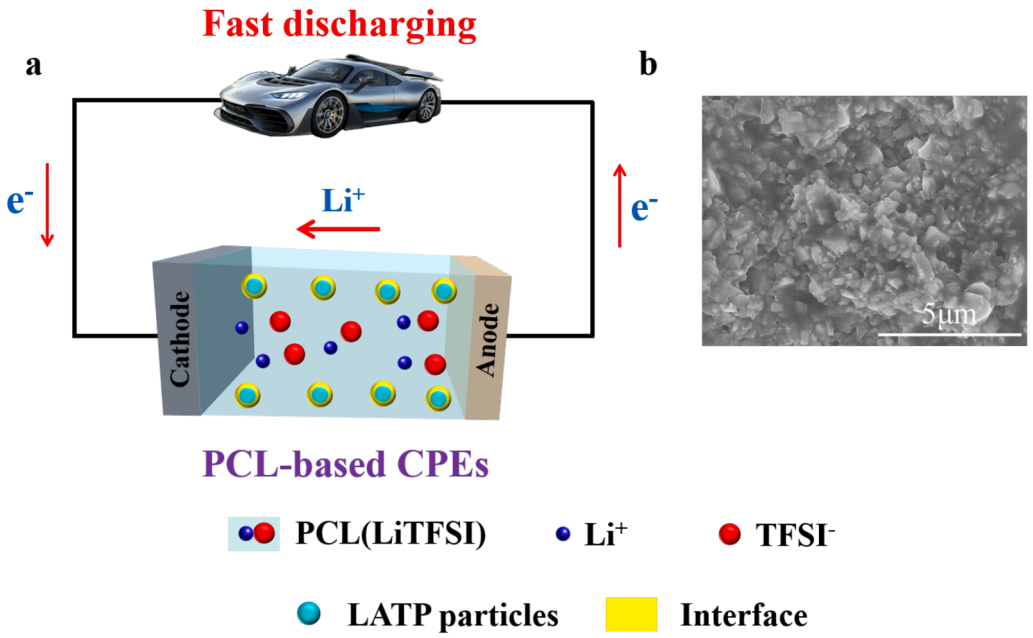

Fig. 1. (a) Schematic illustration of all-solid state lithium battery design with rapid charging/discharging. (b) SEM image of PCL-based CPEs.

two polymers possessed excellent thermal stability for satisfying practical application as CPEs. Differential scanning calorimetry measurements are employed to investigate the amorphousness behavior (Fig. S2d-f). The melting temperature of PCL-based CPEs is distinctively declining because of inhibition crystallinity of polymer after adding LiTFSI and LATP (Fig. S2f). The percentage of crystallinity (χ_c) of PCL, PEO, PCL-based CPEs, and PEO-based CPEs are 41.33%, 61.44%, 25.19%, 51.62%, respectively. The melting heat (ΔH_m) and corresponding χ_c of PCL, PEO, PCL-based CPEs and PEO-based CPEs, and the results of X-ray diffraction (XRD) are shown in Table S1 and Fig. S3. It is noted that the migration of Li-ion is happening in non-crystalline phase [7,40], increasing the proportion of amorphous regions to improve

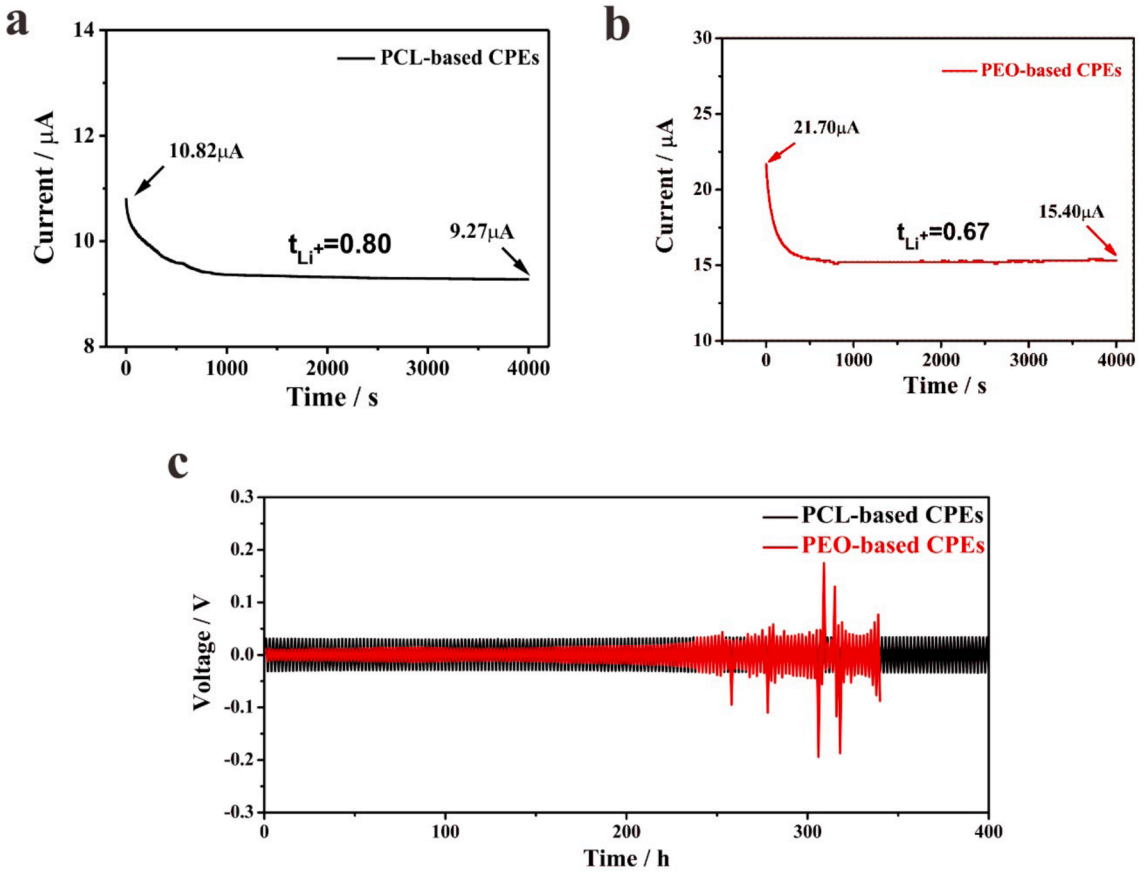

Fig. 2. (a, b) The chronoamperometry profiles of PCL-based CPEs and PEO-based CPEs. (c) Polarization voltage profiles of the symmetrical Li/CPEs/Li cells.

electrochemical properties of CPEs.

3.2. Electrochemical performance of CPEs

The t_{Li}^{+} is a significant influencing factor for CPEs and ASSLBs [41]. A high t_{Li}^{+} of the electrolytes can suppress lithium dendrites by alleviating anion depletion-induced large electric fields near the lithium metal anode [42]. The t_{Li}^{+} of the PCL-based CPEs is 0.8, in contrast to the 0.67 values with PEO-based CPEs in Fig. 2a and b, and the t_{Li}^{+} is calculated as shown in Fig. S4 and Table S2. The high t_{Li}^{+} of PCL-based CPEs is due to the lower crystallinity and optimized content of LATP. Considering the Newman's original LIBs models, electrolytes with modestly higher t_{Li}^{+} would allow higher power densities and enable faster charging (≥2C), even if their conductivity is substantially lower than that of conventional organic liquid electrolytes [15,43,44].

The ionic conductivities of PCL-based and PEO-based CPEs are shown in Fig. S5a and b, which exhibit the ionic conductivity evolution of the CPEs with the change of temperature. The activation energies of PCL-based and PEO-based CPEs are 0.064 eV and 0.081 eV, respectively. The ionic conductivity of PCL-based CPEs is measured to be 0.87×10^{-4} S cm^{-1} at 55 °C, which is lower than that of PEO-based CPEs (1.25×10^{-4} S cm^{-1} at 55 °C). The electrochemical window of CPEs is tested by cyclic voltammetry (CV) and Linear sweep voltammetry (LSV) as illustrated Fig. S5c-f. There is no obvious current increase until 5 V for PCL-based and PEO-based CPEs. Typically, the electrochemical stability window of reported PEO-based electrolyte is in the range from 4 V to 4.7 V. However, with the inorganic fillers are added in PEO-based electrolyte system, the electrochemical stability window of reported PEO-based electrolyte is exceeding 4.8 V, even greater than 5 V [45]. It means that there is no obvious oxidative decomposition of the CPEs with an operating voltage up to 5 V (vs Li/Li^{+}). Therefore, PCL-based and PEO-based CPEs exhibit a wide electrochemical window. Furthermore, to explore the stability of the interface between CPEs and lithium metal anode at high current density, and the symmetric batteries of PCL-based and PEO-based CPEs is tested by different current density (0.12 mA cm^{-2} and 0.25 mA cm^{-2}), at 55 °C. The results of constant current polarization are shown in Fig. S6 and Fig. 2c, and it do not show big difference for PCL-based and PEO-based CPEs at 0.12 mA cm^{-2} after 250 h (Fig. S6), but when current density is increased to 0.25 mA cm^{-2}, the polarization potential of PEO-based CPEs change obviously as exhibited in Fig. 2c. Although the polarization potential of PCL-based CPEs display bigger than that of PEO-based CPEs at initial cycles, the PCL-based CPEs have remarkable interfacial stability and compatibility with lithium anode in long-term cycle, especially at big current density, and forecasting that the PCL-based CPEs is beneficial to alleviating ohmic polarization and concentration polarization, thereby suppressing the lithium dendrite formation in ASSLBs [31].

3.3. Battery performance

To study practical applicability of ASSLBs using PCL-based and PEO-based CPEs, the electrochemical performance of ASSLBs including a

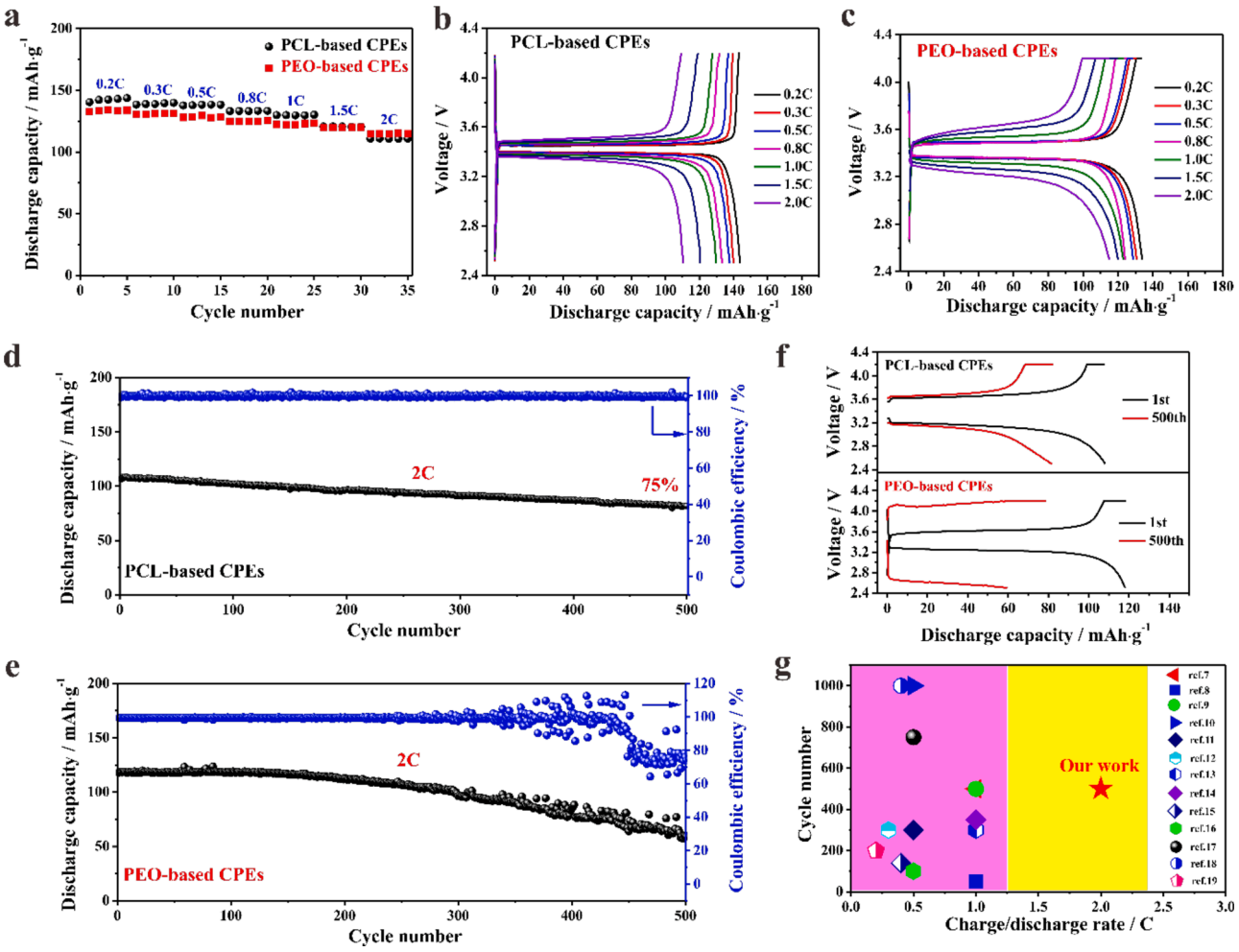

Fig. 3. (a) Rate performance PCL-based CPEs and PEO-based CPEs. (b, c) Typical charging/discharging curves of PCL-based CPEs and PEO-based CPEs at various rates. (d, e) Cycling performance of PCL-based CPEs and PEO-based CPEs. (f) Typical charge/discharge curves of battery with CPEs at different cycles. (g) Comparison of cycling performance of various polymer-based electrolytes.

lithium metal anode and LFP cathode are evaluated. The PCL-based CPEs ASSLBs cycling at different rates are exhibited in Fig. 3a, and display the discharge capacities of 143.7, 139.8, 137.8, 133.4, 129.7, 120.6 and 110.7 mAh g^{-1} at the discharge rates of 0.2, 0.3, 0.5, 0.8, 1, 1.5, and 2 C, respectively. In comparison, the ASSLBs based on PEO-based CPEs ASSLBs exhibit discharge capacities of 134, 131.5, 129.6, 125.4, 123.1, 120.1 and 115.2 mAh g^{-1} at the corresponding rates (Fig. 3a). The typical charging/discharging curves of PCL-based and PEO-based ASSLBs at various rates from 0.2 to 2 C at 55 °C are shown in Fig. 3b and c, and the rate performance curves of PEO-based CPEs show smoother than PCL-based CPEs and higher discharge capacity at 2 C. Additionally, the cycling performance of ASSLBs based on PCL-based CPEs and PEO-based CPEs at 2 C is presented in Fig. 3d and e. The ASSLBs based on PCL-based CPEs exhibit a high initial discharge capacity of 108.2 mAh g^{-1} and remarkable cycling performance with the favorable capacity retention of 75% after ultralong 500 cycles at 2 C (55 °C) as shown in Fig. 3d. Also, throughout 500 cycles, the ASSLBs maintain high and stable Coulombic efficiency values of 99∼100%. In contrast, PEO-based ASSLBs have a higher initial discharge capacity of 118.5 mAh g^{-1} and the Coulombic efficiency show a lot of volatility after 300 cycles with the capacity retention of 50.5% after 500 cycles at 2 C (55 °C) in Fig. 3e. The ionic conductivity of PEO-based CPEs play an important role in rate changing in initial cycle or in short-term cycle. t_{Li}^{+} is a significant factor to impact ASSLBs charging/discharging process and long-term cycling stability [15]. It is shown that the improvements of t_{Li}^{+} would be favorable, particularly allowing a higher attainable state of charging and discharging in practical application, where a large, constant current would be necessary to quickly charging/discharging for the battery. The typical charge-discharge curves of 1st, 500th cycle of the PCL-based CPEs and PEO-based CPEs are exhibited in Fig. 3f. Furthermore, the electrochemical impedance spectroscopy (EIS) curves of PCL-based CPEs and PEO-based CPEs before and after cycling are shown in Fig. S7, the resistance of PCL-based CPEs is increasing from ∼550 Ω to ∼4000 Ω, and the resistance of PEO-based CPEs before and after cycling is ∼600 Ω and ∼6000 Ω, respectively. The cycling performance of ASSLBs based on PCL-based CPEs is superior to those based on PEO-based CPEs ASSLBs recently reported in terms of charge/discharge rate, listed in Fig. 3g and comparison of cycling performance of various PEO-based electrolytes in the terms of charge/discharge rate for ASSLBs in this work. Further details are included in Table S3. It is noted that our result shows excellent cycle performance and the ability of charging/discharging. ASSLBs based on PCL-based CPEs showed good cycling performance (500 cycles) and high capacity retention (75%). And even at 3 C (≈0.43 mA cm^{-2}), it still delivered good cycling performance (500 cycles) and high capacity retention (71%) as shown in Fig. S8. In addition to LFP, $LiNi_{0.5}Mn_{0.2}Co_{0.3}O_2$ and $LiFe_{0.5}Mn_{0.5}PO_4$ are also used as the cathode for ASSLBs with PCL-based CPEs, and the ASSLBs based on $LiNi_{0.5}Mn_{0.2}Co_{0.3}O_2$ exhibits initial discharge capacities of 129.1 mAh g^{-1} at the charging/discharging rates of 0.1 C as exhibited in Fig. S9, the ASSLBs based on $LiFe_{0.5}Mn_{0.5}PO_4$ display high discharge capacities of 120.2 mAh g^{-1} at the charging/discharging rates of 0.1 C as shown in Fig. S10, and high capacity retention (90.6%) after nearly 200 cycles at 0.5 C.

3.4. Interfaces between electrolyte and electrodes in ASSLBs

In order to explore the lithium dendrite formation of interface between lithium metal anode and PCL-based CPEs, and the ASSLBs are disassembled in an Ar-filled glove box after long cycling. The interface of lithium metal anode is observed evidently without lithium dendrites formation as exhibited in Fig. S11. Furthermore, the interface of lithium metal anode is shown in Fig. S11a and b, and the additional EDS mappings of the interface reveal homogenous distributions of various elements (C, O, S, P, Al, Ti) in the Fig. S12. The PCL-based CPEs not only suppress the formation of lithium dendrites in faster charging/discharging process, but also optimize wetting and stability of the interface with lithium metal anode. The stable interface contact and favorable wetting ability are contributing to Li-ion migration and reduce impedance of charge transfer.

To examine the interfacial reactions of ASSLBs based on PCL-based CPEs after 500 cycles, X-ray photoelectron spectroscopy (XPS) is performed to investigate the components and chemical states of the solid electrolyte interphase (SEI) layer between lithium metal anode and CPEs. In the F 1s spectrum, an obvious LiF (684.1 eV) and C-F (688.2 eV) can be detected in Fig. 4a, and LiF can effectively protect lithium metal anode by preventing the electrons from crossing the SEI layer [46]. The formation of LiF can be due to the reaction of metallic Li with PCL-based CPEs, which is believed to be responsible for the stable Li-ion deposition and the outstanding interfacial properties, preventing the dendrite growth and pulverization of the lithium metal anode [47]. The results just have shown the information about the relative composition of the SEI, not the absolute amount of components present. In the C 1s spectrum, it can be detected four peaks with assignments of C-C/C-H (284.5 eV), C-O (286.4 eV), C=O (287.6 eV), COOLi (289.2 eV) as shown in Fig. 4b [48,49]. As for the O 1s spectrum, two peaks are detected at lower binding energy of ∼533.2 eV and ∼533.5 eV [46]. Firstly, it may be oxygen atoms bound to carbon with a double bond or Li_2CO_3. Secondly, oxygen bound to carbon with a single bond at ∼533.5 eV (Fig. 4c) [50]. These two compounds are the reaction products of metallic Li with PCL-based CPEs after long-term cycling. The PCL-based CPEs degradation products of Li_2SO_3 (∼166.2 eV) and Li_3N (∼392.2 eV) in charging/discharging cycles that can be observed in S $2p^{3/2}$ and N 1s spectra as illustrated in Fig. S13. The increased organic component may be contributed to improved Li metal anode morphology and cycling efficiency in the ASSLBs [51]. The inorganic components, especially the LiF, lead to the generation of uniform diffusion field gradients which afford uniform lithium plating [47]. Thus, the ASSLBs based on PCL-based CPEs with the excellent cycling performance and capacity retention have an SEI composed of both organic components and inorganic components to maintain the interface stability. In comparison to PCL-based CPEs, PEO-based CPEs exhibit the same composition of the SEI, but the peaks of LiF, COOLi and Li_2CO_3 are much weaker as shown Fig. 4d–f, indicating that the SEI of PEO-based CPEs cannot maintain cycling performance and cycling efficiency in high charging/discharging rate and high temperature. The unstable SEI of PEO-based CPEs causes the poor cycling performance, low efficiency and capacity retention.

The atomic force microscopy (AFM) images are exhibited in Fig. 5a–c and d–f. The Young's Modulus of PCL-based CPEs and PEO-based CPEs are 2.8 Gpa and 0.63 GPa, respectively. The difference is more clear in corresponding histogram distribution as presented in Fig. S14. Compared with PEO-based CPEs, PCL-based CPEs exhibit a higher Young's Modulus, which makes it possible to suppress or moderate the lithium dendrites formation or growth. In addition, the Young's Modulus of CPEs is a useful property that describes how well an electrolyte can resist non-equilibrium mechanical strains, good Young's Modulus can experience mechanical stresses that can govern battery performance and lifetime [52]. A higher Young's Modulus provides a measure of resilience to dendrite growth. The regions showing a higher Young's Modulus also exhibit relatively higher adhesion properties. The good interfacial properties (adhesion and Young's Modulus) maintain good electrochemical performance in ASSLBs with CPEs. Compared with PEO-based CPEs, PCL-based CPEs exhibit a higher Young's Modulus which can better inhibit the growth of dendrites [53]. During the cycle, small protrusions will be formed at the interface due to the uneven deposition of lithium ions, a soft CPEs separator is beneficial for maintaining good elastic solid-solid interfacial contact, stability with the electrodes upon cycling and lowering the interfacial resistance [26,54], which prevents uneven deposition of Li-ion caused by deformation in charging/discharging process and maintains a stable SEI as shown in Fig. 6a, b [55,56]. Moreover, the lower Young's Modulus will produce low mechanical stress and cannot alleviate the exchange current density

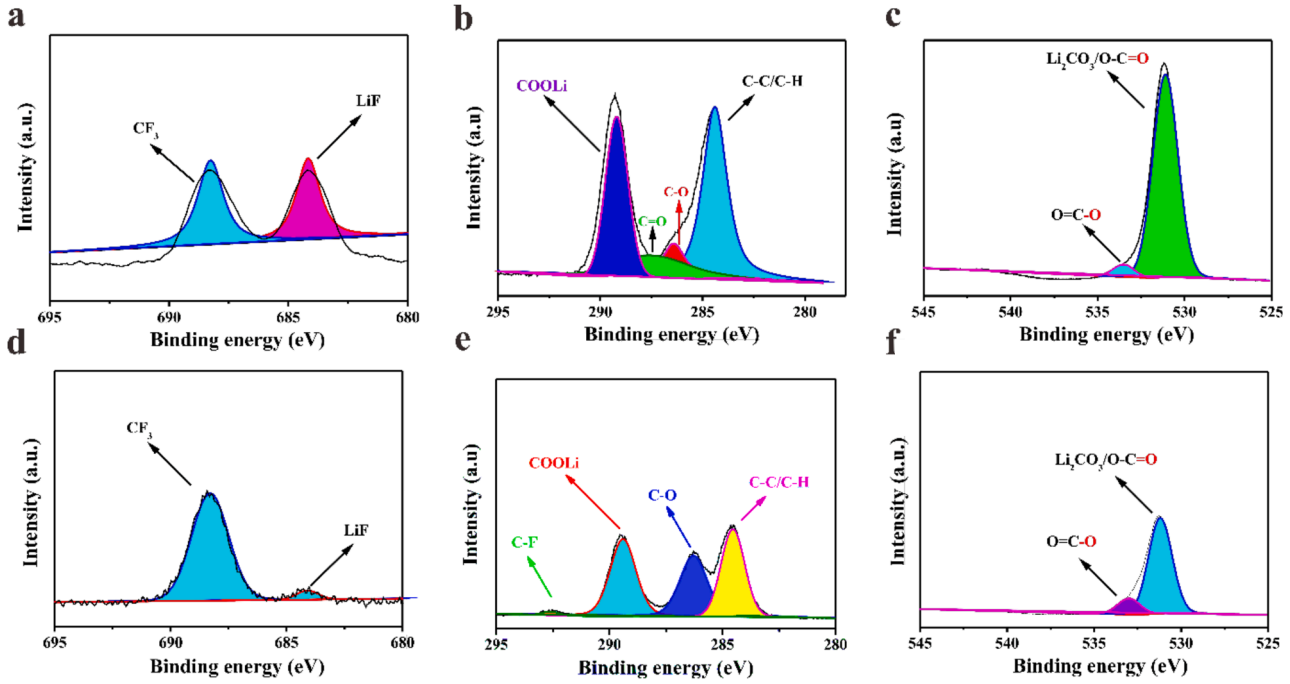

Fig. 4. XPS characterization of SEI formed on lithium metal anode based on PCL-based CPEs after long-term cycling. (a) F 1s, (b) C 1s, (c) O 1s. XPS characterization of SEI formed on lithium metal anode based on PEO-based CPEs after long-term cycling. (d) F 1s, (e) C 1s, (f) O 1s.

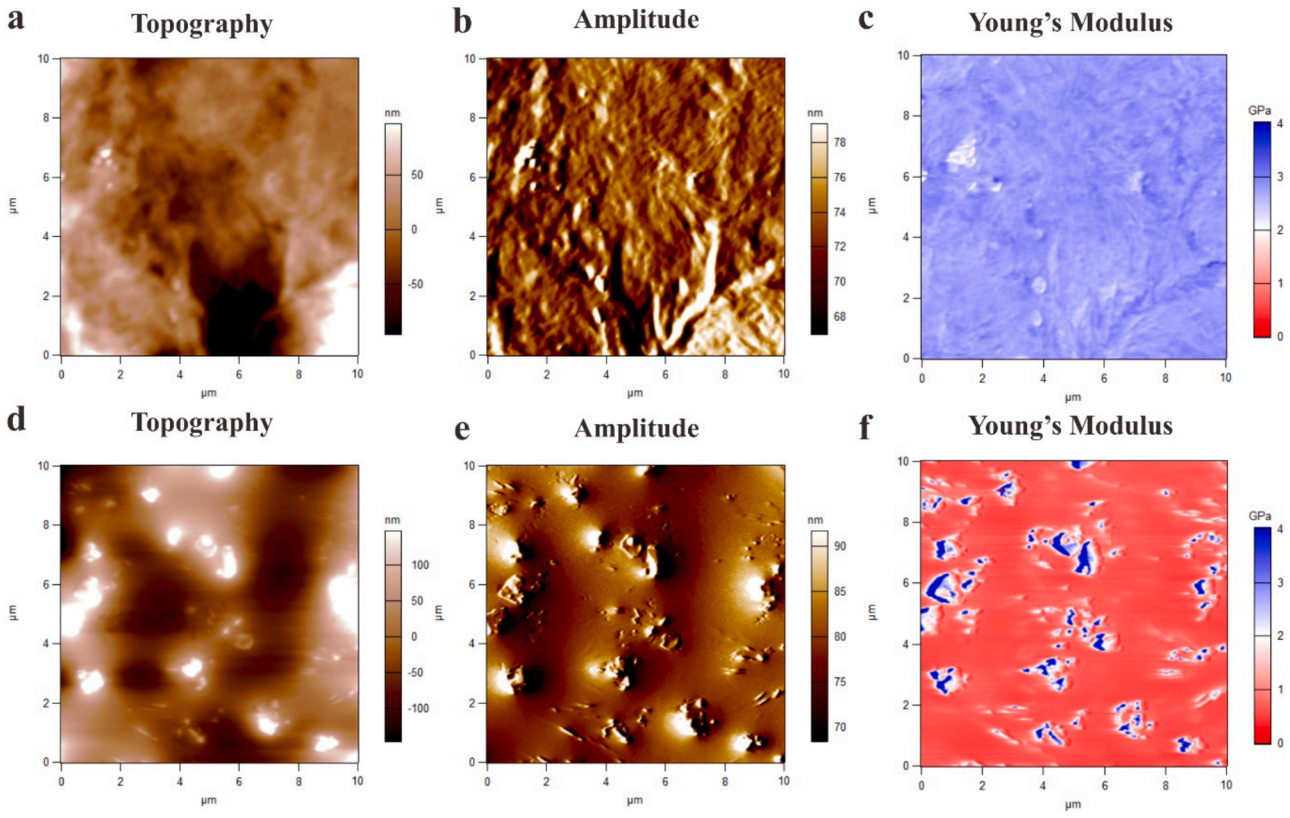

Fig. 5. AFM images of PCL-based CPEs: (a) topography, (b) amplitude, (c) Young's Modulus. AFM images of PEO-based CPEs: (d) topography, (e) amplitude, (f) Young's Modulus.

at the protrusions, and at the same time plastic deformation of lithium metal results in formation the dendritic protrusion as exhibited in Fig. 6c [19,20].

4. Conclusions

In summary, the LFP-based ASSLBs with the PCL-based CPEs show high initial discharge specific capacity of 108.2 mAh g^{-1} with an

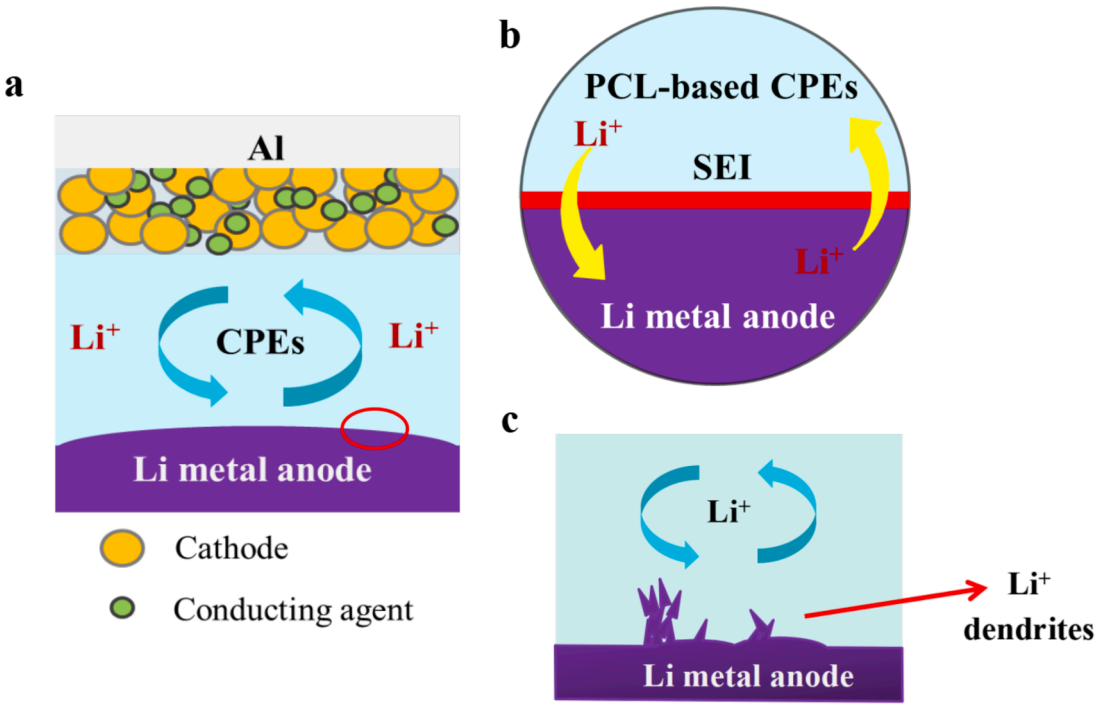

Fig. 6. (a) Physical mechanism of ASSLBs based on PCL-based CPEs. (b) Schematic of a designed PCL-based CPEs with a stable SEI form a red region in (a). (c) Schematic of Li dendrite growth of typical ASSLBs.

excellent capacity retention of 75% after 500 cycles at 2 C and superior rate performance from 0.2 to 2 C (55 °C). The Li symmetric battery with PCL-based CPEs maintains a stable interfacial contact after cycling for 400 h under a current density of 0.25 mA cm^{-2}. The PCL-based CPEs have a high t_{Li}^{+} of 0.8, and suppress the formation of lithium dendrites during cycling, which ensures the transport pathway of Li-ion stable plating/stripping between the CPEs and both electrodes. The characterization CPEs and lithium metal anode indicates that inorganic component and organic component in SEI is formed, which is conducive to long-term cycling in faster charging/discharging process. Besides, the high Young's Modulus of PCL-based CPEs (2.8 GPa) is good for long-term cycling and suppressing the dendrite formation.

CRediT authorship contribution statement

Yuhang Li: Conceptualization, Methodology, Software, Data curation, Formal analysis, Visualization, Writing – original draft. **Fang Wang:** Resources, Visualization, Data curation. **Boyuan Huang:** Writing – review & editing. **Can Huang:** Resources, Data curation. **Dexuan Pei:** Resources, Data curation. **Zixian Liu:** Resources, Data curation. **Shuoguo Yuan:** Visualization, Writing – review & editing. **Shuen Hou:** Supervision. **Guozhong Cao:** Supervision. **Hongyun Jin:** Visualization, Writing – review & editing, Validation, Investigation, Supervision, Project administration, Funding acquisition.

Declaration of Competing Interest

The authors declare no conflicts of interest.

The authors declare that they have no known competing financial interests or personal relationships that could have appeared to influence the work reported in this paper.

Acknowledgments

Thiswork was financially supported by the National Natural Science Foundation of China (12192213), the Key Research and Development Program of Hubei (2021BAA175), Major Scientific and Technological Innovation in Hubei (2019AAA004), Natural Science Foundation of Guangdong Province (Grant No. 2020A1515110989), Postdoctoral Science Foundation of China (Grant No. 2020M682775).

Supplementary materials

Supplementary material associated with this article can be found, in the online version, at doi:10.1016/j.electacta.2022.140624.

References

[1] J.M. Tarascon, M. Armand, Issues and challenges facing rechargeable lithium batteries, Nature 414 (2001) 359–367.
[2] M. Armand, J.M. Tarascon, Building better batteries, Nature 457 (2008) 653–657.
[3] R.S. Chen, Q.H. Li, X.Q. Yu, L.Q. Chen, H. Li, Approaching practically accessible solid-state batteries: stability issues related to solid electrolytes and interfaces, Chem. Rev. 120 (2020) 6820–6877.
[4] L. Ye, X. Li, A dynamic stability design strategy for lithium metal solid state batteries, Nature 593 (2021) 218–222.
[5] K.J. Kim, M. Balaish, M. Wadaguchi, L. Kong, J.L.M. Rupp, Solid-state Li-metal batteries: challenges and horizons of oxide and sulfide solid electrolytes and their interfaces, Adv. Energy Mater. 11 (2020), 2002689.
[6] H.Y. Huo, Y. Chen, R.Y. Li, N. Zhao, J. Luo, J.G. Pereira da Silva, R. Mücke, P. Kaghazchi, X.X. Guo, X.L. Sun, Design of a mixed conductive garnet/Li interface for dendrite-free solid lithium metal batteries, Energy Environ. Sci. 13 (2019) 127–134.
[7] Y.H. Li, M. Liu, S.S. Duan, Z.X. Liu, S.E. Hou, X.C. Tian, G.Z. Cao, H.Y. Jin, A high-voltage hybrid solid electrolyte based on polycaprolactone for high-performance all-solid-state flexible lithium batteries, ACS Appl. Energy Mater. 4 (2021) 2318–2326.
[8] Y. Huang, B. Chen, J. Duan, F. Yang, T.R. Wang, Z.F. Wang, W.J. Yang, C.C. Hu, W. Luo, Y.H. Huang, g-C_3N_4: an interface enabler for solid-state lithium metal batteries, Angew. Chem. Int. Ed. 59 (2019) 3699–3704.
[9] Q.S. Wang, L.H. Jiang, Y. Yu, J.H. Sun, Progress of enhancing the safety of lithium ion battery from the electrolyte aspect, Nano Energy 55 (2019) 93–114.
[10] D. Di Lecce, L. Carbone, V. Gancitano, J. Hassoun, Rechargeable lithium battery using non-flammable electrolyte based on tetraethylene glycol dimethyl ether and olivine cathodes, J. Power Sources 334 (2016) 146–153.
[11] S. Hess, M. Wohlfahrt-Mehrens, M. Wachtler, Flammability of Li-ion battery electrolytes: flash point and self-extinguishing time measurements, J. Electrochem. Soc. 162 (2015) A3084–A3097.
[12] X. Tang, D. Zhou, P. Li, X. Guo, C.Y. Wang, F.Y. Kang, B.H. Li, G.X. Wang, High-performance quasi-solid-state MXene-based Li-I batteries, ACS Cent. Sci. 5 (2019) 365–373.

[13] J.W. Liang, X.N. Li, Y. Zhao, L.V. Goncharova, G.M. Wang, K.R. Adair, C.H. Wang, R.Y. Li, Y.C. Zhu, Y.T. Qian, L. Zhang, R. Yang, S.G. Lu, X.L. Sun, *In situ* Li_3PS_4 solid-state electrolyte protection layers for superior long-life and high-rate lithium-metal anodes, Adv. Mater. 30 (2018), 1804684.

[14] D. Zhou, A. Tkachevaa, X. Tang, B. Sun, D. Shanmukaraj, P. Li, F. Zhang, M. Armand, G.X. Wang, Stable conversion chemistry-based lithium metal batteries enabled by hierarchical multifunctional polymer electrolytes with near-single ion conduction, Angew. Chem. Int. Ed. 58 (2019) 6001–6006.

[15] K.M. Diederichsen, E.J. McShane, B.D. McCloskey, Promising routes to a high Li^+ transference number electrolyte for lithium ion batteries, ACS Energy Lett. 2 (2017) 2563–2575.

[16] J. Xiao, How lithium dendrites form in liquid batteries, Science 366 (2019) 426–427.

[17] C. Monroe, J. Newman, The impact of elastic deformation on deposition kinetics at lithium/polymer interfaces, J. Electrochem. Soc. 152 (2005) A396–A404.

[18] X.M. Hao, J. Zhu, X. Jiang, H.T. Wu, J.S. Qiao, W. Sun, Z.H. Wang, K.N. Sun, Ultrastrong polyoxyzole nanofiber membranes for dendrite-proof and heat-resistant battery separators, Nano Lett. 16 (2016) 2981–2987.

[19] J. Shim, H.J. Kim, B.G. Kim, Y.S. Kim, D.G. Kim, J.C. Lee, 2D boron nitride nanoflakes as a multifunctional additive in gel polymer electrolytes for safe, long cycle life and high rate lithium metal batteries, Energy Environ. Sci. 10 (2017) 1911–1916.

[20] K.R. Deng, J.X. Qin, S.J. Wang, S. Ren, D.M. Han, M. Xiao, Y.Z. Meng, Effective suppression of lithium dendrite growth using a flexible single-ion conducting polymer electrolyte, Small 14 (2018), 1801420.

[21] H. Zhang, C. Li, M. Piszcz, E. Coya, T. Rojo, L.M. Rodriguez-Martinez, M. Armand, Z. Zhou, Single lithium-ion conducting solid polymer electrolytes: advances and perspectives, Chem. Soc. Rev. 46 (2017) 797–815.

[22] Y. Horowitz, M. Lifshitz, A. Greenbaum, Y. Feldman, S. Greenbaum, A.P. Sokolov, D. Golodnitsky, Review-polymer/ceramic interface barriers: the fundamental challenge for advancing composite solid electrolytes for Li-ion batteries, J. Electrochem. Soc. 167 (2020), 160514.

[23] A. Banerjee, X. Wang, C. Fang, E.A. Wu, Y.S. Meng, Interfaces and interphases in all-solid-state batteries with inorganic solid electrolytes, Chem. Rev. 120 (2020) 6878–6933.

[24] D. Zhou, D. Shanmukaraj, A. Tkacheva, M. Armand, G.X. Wang, Polymer electrolytes for lithium-based batteries: advances and prospects, Chem 5 (2019) 2326–2352.

[25] S. Li, S.Q. Zhang, L. Shen, Q. Liu, J.B. Ma, L W, Y.B. He, Q.H. Yang, Progress and perspective of ceramic/polymer composite solid electrolytes for lithium batteries, Adv. Sci. 7 (2020), 1903088.

[26] L.Z. Fan, H. He, C.W. Nan, Tailoring inorganic-polymer composites for the mass production of solid-state batteries, Nat. Rev. Mater. 6 (2021) 1003–1019.

[27] J.X. Zhang, N. Zhao, M. Zhang, Y.Q. Li, P.K. Chu, X.X. Guo, Z.F. Di, X. Wang, H. Li, Flexible and ion-conducting membrane electrolytes for solid-state lithium batteries: dispersion of garnet nanoparticles in insulating polyethylene oxide, Nano Energy 28 (2016) 447–454.

[28] D.E. Fenton, J.M Parker, P.V. Wright, Complexes of alkali metal ions with poly (ethylene oxide), Polymer 14 (1973) 589.

[29] C. Bai, Z. Wu, W. Xiang, G. Wang, Y. Liu, Y. Zhong, B. Chen, R. Liu, F. He, X. Guo, Poly(ethylene oxide)/Poly(vinylidene fluoride)/$Li_{6.4}La_3Zr_{1.4}Ta_{0.6}O_{12}$ composite electrolyte with a stable interface for high performance solid state lithium metal batteries, J. Power Sources 472 (2020), 228461.

[30] Y.H. Li, Z.J. Sun, D.Y. Liu, Y.Y. Gao, Y.K. Wang, H.T. Bu, M.T. Li, Y.F. Zhang, G. X. Gao, S.J. Ding, A composite solid polymer electrolyte incorporating MnO_2 nanosheets with reinforced mechanical properties and electrochemical stability for lithium metal batteries, J. Mater. Chem. A 8 (2020) 2021–2032.

[31] P. Fan, H. Liu, V. Marosz, N.T. Samuels, S.L. Suib, L. Sun, L. Liao, High performance composite polymer electrolytes for lithium-ion batteries, Adv. Funct. Mater. 31 (2021), 2101380.

[32] J.N. Liang, D.C. Chen, K. Adair, Q. Sun, N.G. Holmes, Y. Zhao, Y.P. Sun, J. Luo, R. Y. Li, L. Zhang, S.Q. Zhao, S.G. Lu, H. Huang, X.X. Zhang, C.V. Singh, X.L. Sun, Insight into prolonged cycling life of 4 V all-solid-state polymer batteries by a high-voltage stable binder, Adv. Energy Mater. 11 (2020), 2002455.

[33] C.P. Fonseca, S. Neves, Electrochemical properties of a biodegradable polymer electrolyte applied to a rechargeable lithium battery, J. Power Sources 159 (2006) 712–716.

[34] T. Eriksson, J. Mindemark, M. Yue, D. Brandell, Effects of nanoparticle addition to poly(ε-caprolactone) electrolytes: crystallinity, conductivity and ambient temperature battery cycling, Electrochim. Acta 300 (2019) 489–496.

[35] J. Mindemark, B. Sun, E. Törmä, D. Brandell, High-performance solid polymer electrolytes for lithium batteries operational at ambient temperature, J. Power Sources 298 (2015) 166–170.

[36] D.C. Zhang, L. Zhang, K. Yang, H.Q. Wang, C. Yu, D. Xu, B. Xu, L.M. Wang, Superior blends solid polymer electrolyte with integrated hierarchical architectures for all-solid-state lithium-ion batteries, ACS Appl. Mater. Interfaces 9 (2017) 36886–36896.

[37] A. Bergfelt, M.J. Lacey, J. Hedman, C. Sångeland, D. Brandell, T. Bowden, ε-Caprolactone-based solid polymer electrolytes for lithium-ion batteries: synthesis, electrochemical characterization and mechanical stabilization by block copolymerization, RSC Adv. 8 (2018) 16716–16725.

[38] C Zuo, G. Chen, Y. Zhang, H.H. Gan, S.Q Li, L.P. Yu, X.P Zhou, X.L Xie, Z.G. Xue, Poly(ε-caprolactone)-block-poly(ethylene glycol)-block-poly(ε-caprolactone)-based hybrid polymer electrolyte for lithium metal batteries, J. Membr. Sci. 607 (2020), 118132.

[39] S.S. Duan, H.Y. Jin, J.X. Yu, E.N. Esfahani, B. Yang, J. Liu, Y.Z. Ren, Y. Chen, L. H. Lu, X.C. Tian, S.E. Hou, J.Y. Li, Non-equilibrium microstructure of $Li_{1.4}Al_{0.4}Ti_{1.6}(PO_4)_3$ superionic conductor by spark plasma sintering for enhanced ionic conductivity, Nano Energy 51 (2018) 19–25.

[40] Y. Wu, Y. Li, Y. Wang, Q. Liu, Q. Chen, M. Chen, Advances and prospects of PVDF based polymer electrolytes, J. Energy Chem. 64 (2022) 62–84.

[41] J.H. Cha, P.N. Didwal, J.M. Kim, D.R. Chang, C.J. Park, Poly(ethylene oxide)-based composite solid polymer electrolyte containing $Li_7La_3Zr_2O_{12}$ and poly(ethylene glycol) dimethyl ether, J. Membr. Sci. 595 (2019), 117538.

[42] J. Chazalviel, Electrochemical aspects of the generation of ramified metallic electrodeposits, Phys. Rev. A 42 (1990) 7355–7367.

[43] M. Doyle, T.F. Fuller, J. Newman, The importance of the lithium ion transference number in lithium/polymer cells, Electrochim. Acta 39 (1994) 2073–2081.

[44] N.P. Balsara, J. Newman, Relationship between steady-state current in symmetric cells and transference number of electrolytes comprising univalent and multivalent Ions, J. Electrochem. Soc. 162 (2015) A2720–A2722.

[45] H. Xu, P.H. Chien, J. Shi, Y. Li, N. Wu, Y. Liu, Y.Y. Hu, J.B. Goodenough, High-performance all-solid-state batteries enabled by salt bonding to perovskite in poly (ethylene oxide), Proc. Natl. Acad. Sci. U. S. A. 116 (2019) 18815–18821.

[46] B.H. Zhang, Y.L. Liu, X.M. Pan, J. Liu, K. Doyle-Davis, L.Q. Sun, J. Liu, X.F. Jiao, J. Jie, H.M. Xie, X.L. Sun, Dendrite-free lithium metal solid battery with a novel polyester based triblock copolymer solid-state electrolyte, Nano Energy 72 (2020), 104960.

[47] S. Jurng, Z.L. Brown, J. Kim, B.L. Lucht, Effect of electrolyte on the nanostructure of the solid electrolyte interphase (SEI) and performance of lithium metal anodes, Energy Environ. Sci. 11 (2018) 2600–2608.

[48] F. Wu, Q.Z. Zhu, R.J. Chen, N. Chen, Y. Chen, L. Li, Ionic liquid electrolytes with protective lithium difluoro(oxalate)borate for high voltage lithium-ion batteries, Nano Energy 13 (2015) 546–553.

[49] Q. Zhao, X.T. Liu, S. Stalin, K. Khan, L.A. Archer, Solid-state polymer electrolytes with in-built fast interfacial transport for secondary lithium batteries, Nat. Energy 4 (2019) 365–373.

[50] N.W. Li, Y. Shi, Y.X. Yin, X.X. Zeng, J.Y. Li, C.J. Li, L.J. Wan, R. Wen, Y.G. Guo, A flexible solid electrolyte interphase layer for long-life lithium metal anodes, Angew. Chem. Int. Ed. 57 (2018) 1505–1509.

[51] R. Weber, M. Genovese, A.J. Louli, S. Hames, C. Martin, I.G. Hill, J.R. Dahn, Long cycle life and dendrite-free lithium morphology in anode-free lithium pouch cells enabled by a dual-salt liquid electrolyte, Nat. Energy 4 (2019) 683–689.

[52] M.B. Dixit, W. Zaman, N. Hortance, S. Vujic, B. Harkey, F. Shen, W.Y. Tsai, V. De Andrade, X.C. Chen, N. Balke, K.B. Hatzell, Nanoscale mapping of extrinsic interfaces in hybrid solid electrolytes, Joule 4 (2020) 207–221.

[53] C. Deng, N. Chen, C. Hou, H. Liu, Z. Zhou, R. Chen, Enhancing interfacial contact in solid-state batteries with a gradient composite solid electrolyte, Small 17 (2021), 2006578.

[54] D.G.M. Jeffrey Lopez, Y. Cui, Z. Bao, Designing polymers for advanced battery chemistries, Nat. Rev. Mater. 4 (2019) 312–330.

[55] P. Barai, K. Higa, V. Srinivasan, Lithium dendrite growth mechanisms in polymer electrolytes and prevention strategies, Phys. Chem. Chem. Phys. 19 (2017) 20493–20505.

[56] P. Bai, J. Li, F.R. Brushett, M.Z. Bazant, Transition of lithium growth mechanisms in liquid electrolytes, Energy Environ. Sci. 9 (2016) 3221–3229.